applied optics

1.6 kW Yb fiber amplifier using chirped seed amplification for stimulated Brillouin scattering suppression

Jeffrey O. White,[1,*] Mark Harfouche,[2] John Edgecumbe,[3] Naresh Satyan,[4] George Rakuljic,[4] Vijay Jayaraman,[5] Christopher Burgner,[5] and Amnon Yariv[2]

[1]U.S. Army Research Laboratory, 2800 Powder Mill Rd., Adelphi, Maryland 20783-1138, USA
[2]Department of Electrical Engineering, California Institute of Technology, 1200 E. California Blvd., Pasadena, California 91125, USA
[3]Nufern, 7 Airport Park Rd, E. Granby, Connecticut 06026, USA
[4]Telaris, Inc., 2118 Wilshire Blvd. #238, Santa Monica, California 90403, USA
[5]Praevium Research, Inc., 5330 Debbie Rd., Suite 100, Santa Barbara, California 93111, USA
*Corresponding author: jeffrey.o.white@osamember.org

Received 2 August 2016; revised 16 October 2016; accepted 17 October 2016; posted 18 October 2016 (Doc. ID 273015); published 15 November 2016

In a high power fiber amplifier, a frequency-chirped seed interrupts the coherent interaction between the laser and Stokes waves, raising the threshold for stimulated Brillouin scattering (SBS). Moving the external mirror of a vertical cavity surface-emitting diode laser 0.2 μm in 10 μs can yield a frequency chirp of 5×10^{17} Hz/s at a nearly constant output power. Opto-electronic feedback loops can linearize the chirp, and stabilize the output power. The linear variation of phase with time allows multiple amplifiers to be coherently combined using a frequency shifter to compensate for static and dynamic path length differences. The seed bandwidth, as seen by the counter-propagating SBS, also increases linearly with fiber length, resulting in a nearly-length-independent SBS threshold. Experimental results at the 1.6 kW level with a 19 m delivery fiber are presented. A numerical simulation is also presented.

OCIS codes: (060.2320) Fiber optics amplifiers and oscillators; (190.5890) Scattering, stimulated; (140.3518) Lasers, frequency modulated.

http://dx.doi.org/10.1364/AO.56.00B116

1. INTRODUCTION

One obstacle in the scaling of high power fiber lasers arises because of nonlinear effects, e.g., stimulated Brillouin scattering, due to the large intensity × length product. Efforts to raise the power threshold include: (a) reducing the Brillouin gain by combining materials with positive and negative elasto-optic coefficients, [1] or tailoring the acoustic index to avoid guiding the acoustic wave [2,3], (b) reducing the effective Brillouin gain by using a seed linewidth much wider than the Brillouin bandwidth [4,5,6], (c) enlarging the Brillouin bandwidth relative to the seed linewidth [7,8,9], (d) lowering the laser intensity by enlarging the fiber core, and (e) minimizing the required active fiber length by pumping at the wavelength of maximum absorption and doping as heavily as possible. Conventional approaches to broadening the seed linewidth reduce the coherence length making it difficult to coherently combine multiple fiber amplifiers. For example, a seed bandwidth of 40 GHz (coherence length in fiber = 5 mm) will require path length matching of much less than 1 mm to maintain high coherence.

In previous work, we have shown that chirped seed amplification (CSA) in conjunction with acousto-optic frequency shifters and feedback circuitry can maintain coherence between two fiber amplifiers despite path length differences of 10–50 cm [10,11]. The maximum path length difference is limited to $c\Delta\nu_{\max}/\beta n$, where $\Delta\nu_{\max}$ is the maximum available frequency shift, β is the chirp, and c/n is the speed of light in the fiber. It is also limited by the intrinsic coherence length of the unchirped laser. The laser we describe below has an unchirped bandwidth of 40 MHz (FWHM), therefore a coherence length of 5 m.

In a tiled geometry, this ability to control the phase electronically can be used to predistort an emitted wavefront in order to compensate for atmospheric turbulence [12]. CSA also leads to an SBS threshold that is nearly fiber length independent in the long fiber limit. This approach is compatible with the other techniques for suppressing SBS, except those that increase the Brillouin linewidth. The present work describes the use of CSA with a MEMS-VCSEL seed to scale the output

power of a Yb fiber amplifier to 1.6 kW, while at the same time allowing a 19 m delivery fiber. A numerical simulation of the experiment shows that the SBS threshold could be raised to 2 kW by optimizing the pump attenuation.

2. CHIRPED DIODE LASER TECHNOLOGY

Our work with chirped seeds began with a conventional VCSEL in which linear chirps up to 5×10^{15} Hz/s were produced by a time-varying current and an optoelectronic feedback circuit [13]. A 100 × faster chirp can be obtained by moving the external mirror of a MEMS-VCSEL. Our laser is pumped with an 850 nm diode and has a cavity length of 11 μm [14]. The mirror can be moved 1 μm via the Coulomb force by changing the bias by 50 V.

A chirp of 5×10^{17} Hz/s can be obtained by moving the mirror 0.2 μm in 10 μs. A highly linear chirp can be obtained by fine adjustment of the temporal voltage waveform. To maintain a constant seed power during the frequency sweep, the laser output passes through a semiconductor optical amplifier controlled by a feedback loop.

The chirp is determined by passing part of the MEMS-VCSEL output through an unbalanced fiber Mach–Zehnder interferometer (FSR = 71.9 GHz), and calculating the instantaneous frequency of the resultant beat signal. The chirps (measured away from the turning points) are 5.2×10^{16}, 1.0×10^{17}, 2.6×10^{17}, and 5.2×10^{17} ±5% Hz/s for durations of 200, 50, 20, and 10 μs, respectively. The frequency spans are 5.2 THz (∼20 nm at 1.06 μm), limited only by the Yb gain spectrum.

The frequency of the seed can be made to follow a triangular waveform in time, spanning up to 100 nm, larger than the entire Yb gain spectrum [13]. One issue is SBS occurring at the turning points in the waveform, where the chirp passes through zero. We have shown that a dual source combined with an electro-optic switch [15] can solve this problem [11]. In the present work, we alternate between a chirped seed and a conventional broadband seed, injecting the latter at the turning points. This reduces the duty cycle for coherent combining to ∼70%, but it allows us to easily study the behavior of the SBS, without requiring a second chirped source.

3. SBS SUPPRESSION

An intuitive explanation of the SBS suppression due to a chirped seed has been given in our previous work, and a numerical model has shown good agreement with experiment [16]. If the chirp is linear and the Brillouin gain $g(\nu)$ is Lorentzian, the gain for every frequency component of the Stokes wave will follow a Lorentzian in space. The Stokes frequency that comes into resonance in the middle of the fiber will have the largest gain when integrated over z. The full width at half-maximum (FWHM) gain for this component will be $c\Delta\nu_B/(2\beta n)$. For a Brillouin linewidth $\Delta\nu_B = 100$ MHz (FWHM) and a chirp of $\beta = 10^{17}$ Hz/s, this frequency component will experience gain over a distance of only ∼0.1 m.

To estimate the SBS threshold, one needs to look at the gain experienced by all frequencies present during one transit time. In the high chirp limit, the gain spectrum for this ensemble of Stokes frequencies, g_{ens}, is effectively flattened and broadened to $\beta\tau$. While the frequency integral of g_{ens} is unchanged by chirping, a large reduction in Stokes power can be realized because the small signal gain is exponential. A flat spectrum such as this yields the highest threshold for a given spectral width.

4. EXPERIMENT

We injected the seed laser described in Section 2 into a Yb amplifier with a 25 m final stage (Fig. 1). A mode field adapter was located between the tap and the pump combiner. The pump diodes operated at 976 nm with a maximum power of 1.8 kW. The amplifier output is typically limited by SBS in the final stage. The diameters of the core, cladding, low-index polymer, and jacket are: 25/400/450/550 μm. Ninety percent of the pump power is absorbed in the first 5.6 m of the fiber, so our setup is equivalent to having a 19 m delivery fiber. The final stage fiber is non-polarization-maintaining. The first 5 m is wound around a mandrel for cooling and to increase the loss for higher order modes. An endcap was spliced to the fiber and then cleaved to a length of 3.5 mm with an angle of 4.2°.

Three 100 MHz photodiodes monitor the power entering the final stage, the output power, and the backward power leaving the final stage. Mean values were obtained by digitizing and averaging the photodiode output, and calibrating with subkHz bandwidth thermal sensors.

Oscilloscope traces taken with the fast photodiodes at an output power of 1.6 kW are shown in Fig. 2. The output power (top trace) has some unintentional modulation, and transients that occur when switching between the two seeds. This modulation is also present on the power entering the final stage (not shown) and is due to wavelength- and polarization-dependent loss/gain and dispersion in the components following the seed laser, including the electro-optic switch, preamplifier stages, and the taps.

The backward power (bottom trace) has the stochastic behavior characteristic of the initiation from spontaneous scattering. For the two slower chirps, the (+) and (−) chirps yielded the same backward power. For the two faster chirps, at the higher powers, the (+) chirp had significantly more backward power, as shown below. Oscilloscope traces were recorded and

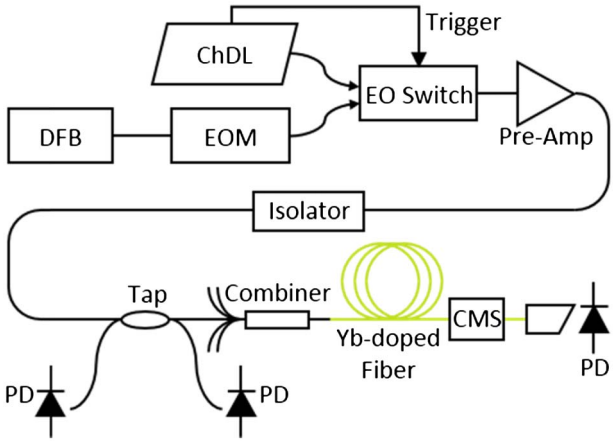

Fig. 1. Experimental setup with chirped diode laser (ChDL), distributed feedback Bragg (DFB) laser, electro-optic modulator (EOM), photodiodes (PD), cladding mode stripper (CMS), and end cap.

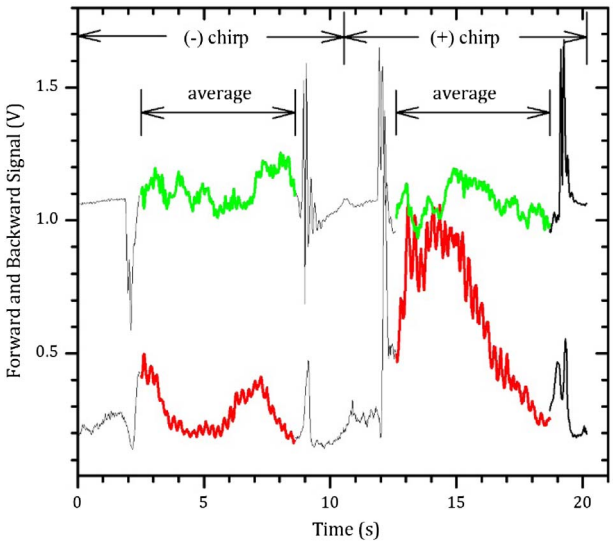

Fig. 2. Oscilloscope traces representing the output power (upper trace) and backward power (lower trace), taken at an output power of 1.6 kW. The data points in Fig. 3 are averages of the bold portions of the traces.

used to obtain the fraction of the backward power due to the (–) chirp.

The output power was varied by changing the current to the diodes pumping the final stage. The backward SBS power can then be plotted versus the output power (Fig. 3). Data for the two slower chirps is an average of (+) and (–) chirp. Data for the two faster chirps are for only the (–) chirp.

Data taken with the 40-GHz seed alone is shown for comparison. We were unable to obtain more than 1.3 kW with the 40-GHz seed because spikes in the backward power would quickly trip the interlock. The highest output with the chirped seed, 1.6 kW, was limited by the available pump power. The

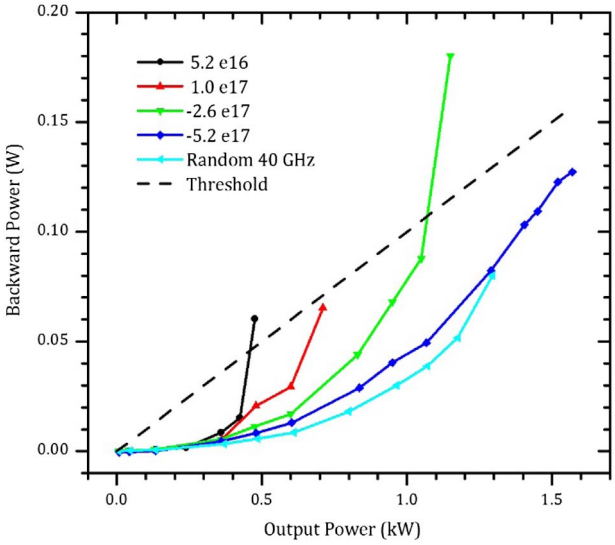

Fig. 3. Backward power versus output power for various chirps, and for a seed with a bandwidth of 40 GHz, produced by random phase modulation. The dashed line represents a ratio of $10^{-4}:1$.

backward power in all cases clearly shows a threshold behavior at the onset of SBS. We define threshold as the point where the backward power equals 10^{-4} times the output power. The threshold output power is increasing approximately linearly with chirp.

We have observed higher SBS for the (+) chirp with other *co-pumped* fiber amplifiers. A natural explanation for this would be that heating of the fiber produces a Brillouin frequency that decreases along the fiber length, so that the Stokes wave stays in resonance with the pump longer. In other words, the backward propagating Stokes wave sees an increase in the Brillouin frequency that offsets the increase in the pump frequency. We have also observed that the (+) chirp yields less SBS with a 500 W *counter-pumped* Yb amplifier. The model described in the next section was developed in part to test this hypothesis.

5. MODELING

The model described previously [16] has been modified to include the effect of temperature on the speed of sound, which in turn affects the Brillouin frequency, bandwidth, and the strength of the thermal phonon "noise" from which the stimulated scattering grows. Changes in the Brillouin frequency are accompanied by changes in the acoustic wave vector, the acousto-optic coefficient, and the elasto-optic coefficient.

Our first step is to find the steady-state solution of the system consisting of pump diode, laser, and Yb inversion, with no: (a) acoustic wave, (b) Stokes wave, or (c) seed modulation. The heat generated inside the fiber is used to calculate the temperature of the core and all of the temperature-dependent quantities. These are used as the initial conditions for solving equations describing the coupling between the modulated laser, Stokes wave, and acoustic field [17]. The assumption of pump waves that are constant in time is valid providing the Stokes wave remains small. In the simulation shown below, the Stokes power is <1% of the pump power throughout the fiber, even at $z = 21$ m, where the ratio is highest. In practical amplifiers, and in the simulations shown below, the backward Stokes power is typically <1% of the seed laser power at the start of the final stage ($z = 0$), where the ratio is highest.

The parameters used in the model are given in Table 1. All are values taken from literature, except that the electrostrictive coefficient had to be multiplied by a factor of five to bring the simulation into agreement with the data. The equations were solved on a grid with intervals related by $\Delta z = c\Delta t/n$. The number of grid points in z is given by $N_z = 8\beta\tau^2$, i.e., approximately 8 × the time-bandwidth product, where the seed bandwidth is taken to be $\beta\tau$ for this purpose. At the highest chirp, the simulation takes 10^3 s on an Intel Xeon 3.3 GHz CPU running Matlab.

The initial conditions for a pump power of 1.8 kW are shown in Figs. 4–6. These conditions are representative of the highest output power data point in Fig. 3.

The fractional inversion has a peak of 0.6 at $z = 0$ and maintains a value of at least 0.012 throughout the fiber because of the small but finite absorption at 1.06 μm (Fig. 5).

The temperature of the core was calculated by solving the radial heat equation, assuming that all of the heat is generated on the axis, and that the interface between the outer plastic

Table 1. Simulation Parameters

Brillouin frequency (at 300 K)	16.2 GHz
Brillouin bandwidth (at 300 K)	58 MHz
Thermal Brillouin Freq. shift	2.25 MHz/K
Silica heat capacity	700 J/(kg K)
Silica thermal conductivity	1.38 W/(mK)
Polymer thermal conductivity	0.2 W/(mK)
Thermal convection coefficient	250 W/(m^2 K)
Ambient temperature	300 K
Fiber attenuation at 976 nm	1.8 dB/m
Yb absorption cross section at 976 nm	10.5×10^{-25} m^2
Yb emission cross section at 976 nm	0.7×10^{-25} m^2
Yb absorption cross section at 1064 nm	0.03×10^{-25} m^2
Yb emission cross section at 1064 nm	2.5×10^{-25} m^2
Yb excited state decay time	1 ms
Electrostrictive coefficient	4.5
Polarization factor	1.0 (linear)

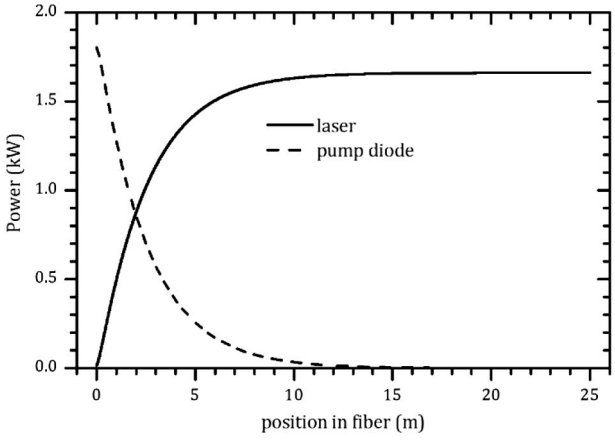

Fig. 4. Pump and laser powers versus position in the fiber at $t = 0$.

surface and the surrounding air is represented by the thermal convection coefficient given above. We have no actual measurements of fiber temperature with which to compare, so this value was chosen to bring the temperature at the glass/plastic interface to a value of ~450 K, at the limit of long-term stability.

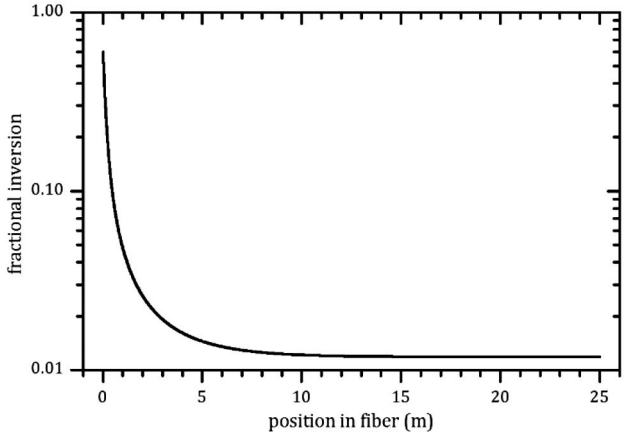

Fig. 5. Fractional inversion versus position in the fiber at $t = 0$, at a pump power of 1.8 kW.

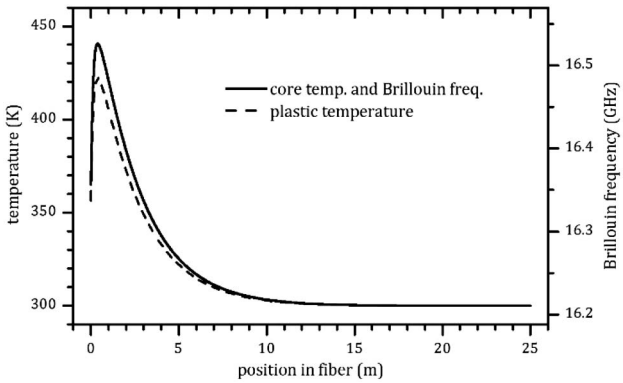

Fig. 6. Simulated conditions inside the fiber at a pump power of 1.8 kW. Temperature at the center of the core (upper curve), at the cladding/coating interface (lower curve). The Brillouin frequency is shown by the solid curve referred to the right-hand axis.

The temperature reaches a peak at 0.4 m into the fiber (Fig. 6), where the Yb ions are cycling the fastest due to a combination of strong pump and stimulated emission. We also show the temperature occurring at the glass/plastic interface, which is the most vulnerable point.

The Brillouin frequency follows the same curve as the core temperature (Fig. 6). The 0.3 GHz variation in ν_B is significant with respect to $\Delta\nu_B$, but it is present only in a short length of fiber, so has a minimal effect on the net Brillouin gain. The effective "chirp" of ν_B is much less than that due to the chirped seed, so we do not expect that temperature will affect the (+) and (–) chirps differently. We have estimated the effect on the Brillouin frequency of the compressive strain induced by the cooler cladding. We adapted an earlier treatment of a fiber at uniform temperature, but where the core and cladding have different coefficients of thermal expansion [18]. Silica is unusual in that the speed of sound decreases with pressure, so the compressive strain lowers the Brillouin frequency. In the conditions discussed here, the effect of strain is minor.

The Brillouin bandwidth measured in a standard optical fiber at 1.32 μm has a small dependence on temperature in the region of 300–400 K [19,20,21]. Lacking data on our particular fiber, we take the bandwidth to be constant at 58 MHz [22].

The results of a simulation of four transits of the fiber for a chirp of $\beta = 5.2 \times 10^{17}$ Hz/s are shown in Fig. 7–10. Longer simulations gave essentially the same results. The z-dependence of the laser power at the end of the last transit is unchanged from that shown in Fig. 4. The z-dependence of the Stokes power at the end of the last transit is shown in Fig. 7. One can see that the Stokes power at $z = 0$ is three to four orders of magnitude larger than the spontaneous level at $z = 25$ m. Even so, the stochastic behavior is dominant, as opposed to the case where the SBS is far above threshold (see, for example, Fig. 1 in Ref. [16]).

In the near-threshold condition, the z-dependence of the magnitude squared density fluctuation also has the random appearance characteristic of the noise throughout most of the fiber (Fig. 8).

The time-dependent results from the simulation are shown in Figs. 9 and 10. Due to the chirp, $|\rho|^2$ averaged over z

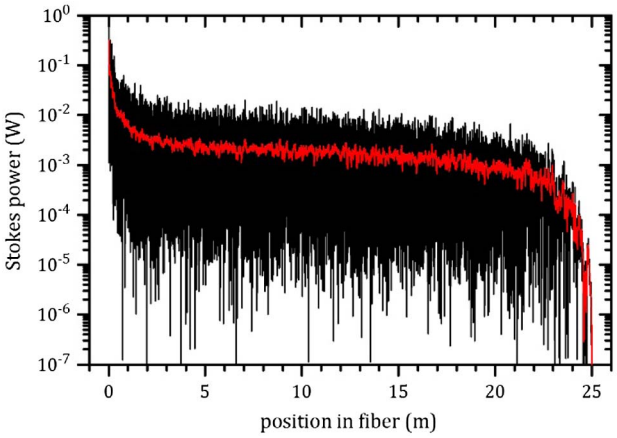

Fig. 7. Stokes power versus position in the fiber versus z, after the last transit, and a sliding average taken over 5 cm.

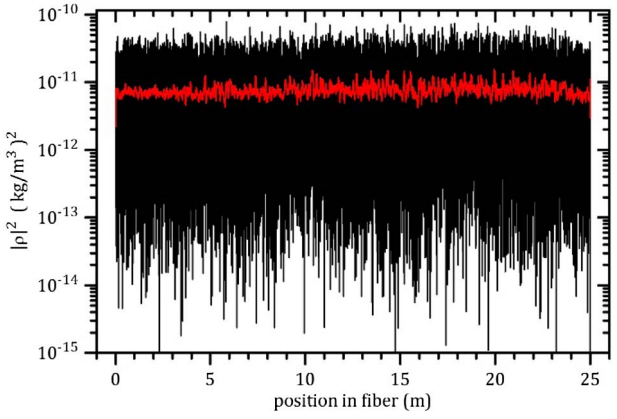

Fig. 8. Magnitude squared density fluctuation versus z, after the last transit, and a sliding average taken over 5 cm.

increases by only three orders of magnitude over the spontaneous level (Fig. 9). The rise time here is approximately one phonon lifetime and shows that the simulation is behaving according to intuition.

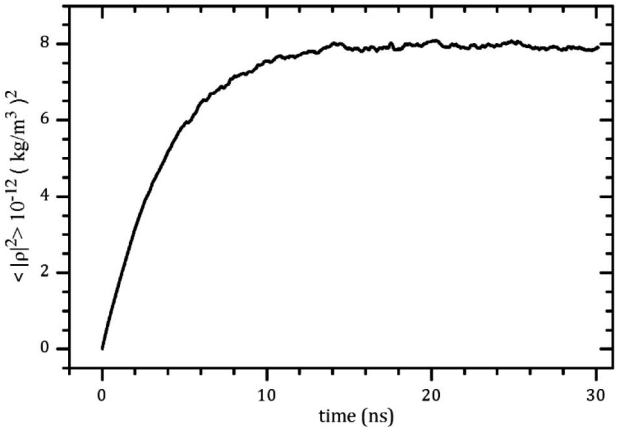

Fig. 9. Magnitude squared density fluctuations averaged over z, versus time, for one quarter of a transit.

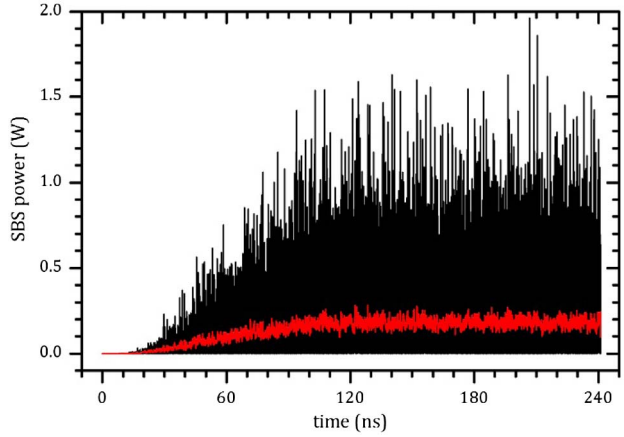

Fig. 10. SBS power at $z = 0$ versus time, for two transits, and a sliding average taken over 0.24 ns.

In these near-threshold conditions, the output laser power (1.66 kW) has temporal fluctuations on the order of only 1%, so we do not show it here. The Stokes power leaving the fiber, P_S $(z = 0)$, reaches a pseudosteady-state within one fiber transit time (Fig. 10).

Knowledge of the peak SBS power is important for protecting upstream components in the amplifier. The statistics are shown on a histogram of the instantaneous SBS power sampled at 2 ps intervals for eight transits (Fig. 11).

A compilation of simulation results is shown in Fig. 12, for comparison with Fig. 3. The average of the Stokes power was taken over the final three transits, to avoid the initial transient. The threshold scales linearly with chirp, in this regime. The effect of neglecting the heating in the fiber and the subsequent shift in Stokes frequency is shown by the square symbols. For these power levels and chirps, neglecting the temperature dependence is of no consequence. For shorter fibers, the suppression of SBS due to a temperature variation is well-known [8]. The large difference between the spatial variation of Brillouin frequency and that of the seed (Fig. 6) suggests that the temperature gradient will not introduce any additional SBS for the (+) chirp, and none was observed in our simulations.

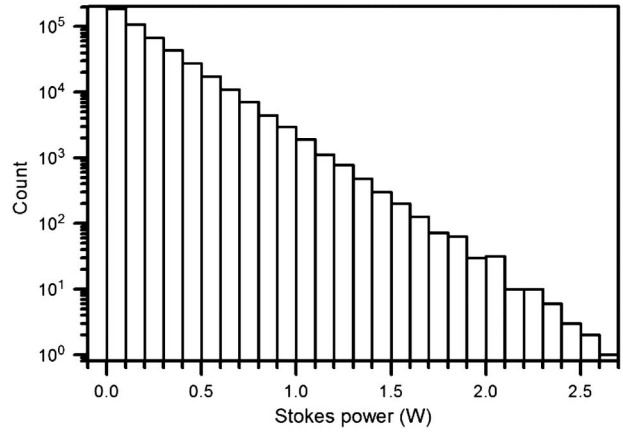

Fig. 11. Histogram of $P_S(z = 0, t)$ sampled at the grid spacing of 2 ps for eight transits. The average power is 0.2 W.

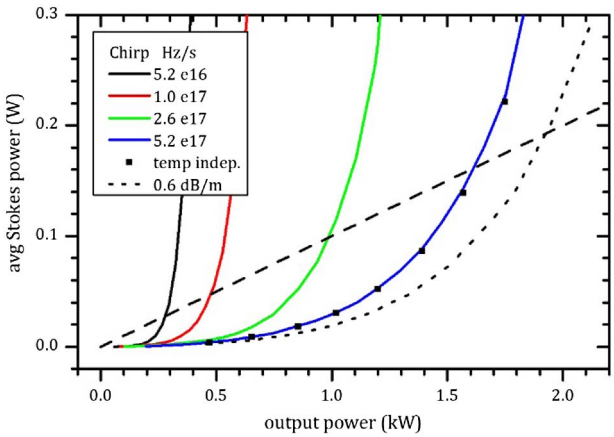

Fig. 12. Average Stokes power versus output laser power calculated for various chirps. The solid lines are calculated with the full temperature dependence. The symbols are calculated as though the entire fiber were at 300 K. The dotted line is calculated at the fastest chirp with a lower pump attenuation of 0.6 dB/m. The dashed line indicates the SBS threshold.

6. DISCUSSION

The experimentally-observed chirp-sign-dependent SBS is not explained by the above simulation. The temperature dependence introduces an effect on the SBS of the correct sign but insufficient magnitude to explain the data. Other sources of chirp-sign-dependent SBS could be the temperature-induced strain caused by a lateral temperature gradient in the fiber. Our estimate of the effect, borrowing from the analysis in Ref. [18], indicates that this is unlikely.

The most likely source of the chirp asymmetry is seeding of the Stokes wave by a Fresnel reflection of the laser from the end-cap [23]. This will occur when $2\beta\tau > \Delta\nu_B$. For a 25 m fiber, this effect will begin to occur for chirps $\beta > 6.6 \times 10^{16}$ Hz/s. The effect was large enough for us to notice at $\beta = 2.6 \times 10^{17}$ Hz/s. The problem can be resolved by reducing the reflections from the end cap, or by using a sawtooth negative chirp, such as in Ref. [11].

The pump wavelength and Yb concentration in the test setup available to us had been chosen to minimize the length of the final stage amplifier, i.e., they were appropriate for minimizing SBS due to a conventional seed. That choice, in combination with the core and cladding diameters, yielded a pump absorption of 1.8 dB/m. With CSA, longer fibers are less of an issue. If the amplifier were optimized for a chirped seed and a long delivery fiber, the optimal pump absorption would be lower, for purposes of lowering the peak fiber temperature and reducing the gIL Brillouin gain product. A simulation of an amplifier with an absorption reduced to 0.6 dB/m shows that the threshold could be raised to 2 kW in this fashion without requiring an increase in chirp (Fig. 12).

Several other engineering steps could be taken to perfect the CSA technique. In the current configuration, the seed power is stabilized with a feedback circuit driven by a photodetector located close to the MEMS-VCSEL. If the power fluctuations at the output of the amplifier (Fig. 2) are a concern, they can be minimized by using for feedback a photodetector located at the amplifier output, or at the tap in Fig. 1. Of course, the bandwidth will be limited by the transit time of the feedback loop.

The same could be said if unwanted phase fluctuations at the output of the amplifier are a concern. In the current configuration, the linear chirp is produced by a feedback circuit that samples the phase of the MEMS-VCSEL. Propagation through dispersive elements will reduce the linearity, and degrade the coherent combining of multiple amplifiers. Nonlinearities in the output chirp can also be minimized by extending the feedback circuit to incorporate the entire chain.

Designing an amplifier specifically for use with a chirped seed would begin with a measurement of the wavelength- and polarization-dependent dispersion and gain of the components in the amplifier chain. Based on those results, one can design or select broadband components that are wavelength independent over a 20 nm range, or that compensate for each other over that range, for example.

7. CONCLUSIONS

We have demonstrated that a 1 mW 1.06 μm MEMS-VCSEL can be scaled with a Yb fiber amplifier to the multi-kW level using CSA. The significance of a linearly chirped seed is that it allows multiple amplifiers to be coherently combined without strict path length matching, and that it allows long delivery fibers. Our setup is equivalent to a 19 m delivery fiber. Our 1.6 kW result is the most power so far transmitted through a large mode area fiber of such length. A simulation indicates that 2 kW could be obtained from a 25 m amplifier if the pump attenuation were optimized.

Funding. High Energy Laser Joint Technology Office (13-SA-0509); U.S. Army Research Office (ARO) (W911NF-11-2-0081).

REFERENCES AND NOTES

1. P. D. Dragic, J. Ballato, S. Morris, and T. Hawkins, "Pockels' coefficients of alumina in aluminosilicate optical fiber," J. Opt. Soc. Am. B **30**, 244–250 (2013).
2. A. Kobyakov, S. Kumar, D. Q. Chowdhury, A. B. Ruffin, M. Sauer, S. R. Bickham, and R. Mishra, "Design concept for optical fibers with enhanced SBS threshold," Opt. Express **13**, 5338–5346 (2005).
3. C. Robin, I. Dajani, and F. Chiragh, "Experimental studies of segmented acoustically tailored photonic crystal fiber amplifier with 494 W single-frequency output," Proc. SPIE **7914**, 79140B (2011).
4. L. Yingfan, L. Zhiwei, D. Yongkang, and L. Qiang, "Research on SBS suppression based on multi-frequency phase modulation," Chin. Opt. Lett. **7**, 29–31 (2009).
5. J. Edgecumbe, T. Ehrenreich, C.-H. Wang, K. Farley, J. Galipeau, R. Leveille, D. Björk, I. Majid, and K. Tankala, Solid State and Diode Laser Technical Review, 17 June 2010.
6. D. Brown, M. Dennis, and W. Torruellas, "Improved phase modulation for SBS mitigation in kW-class fiber amplifiers," in *SPIE Photonics West*, San Francisco, California, 24 January 2011.
7. K. Shiraki, M. Ohashi, and M. Tateda, "Performance of strain-free stimulated Brillouin scattering suppression fiber," J. Lightwave Technol. **14**, 549–554 (1996).
8. J. Hansryd, F. Dross, M. Westlund, P. Andrekson, and S. Knudsen, "Increase of the SBS threshold in a short highly nonlinear fiber by applying a temperature distribution," J. Lightwave Technol. **19**, 1691–1697 (2001).

9. J. Boggio, J. Marconi, and F. Fragnito, "Experimental and numerical investigation of the SBS-threshold increase in an optical fiber by applying strain distributions," J. Lightwave Technol. **23**, 3808–3814 (2005).
10. A. Vasilyev, E. Petersen, N. Satyan, G. Rakuljic, A. Yariv, and J. O. White, "Coherent power combining of chirped-seed Erbium-doped fiber amplifiers," IEEE Photon. Technol. Lett. **25**, 1616–1618 (2013).
11. J. O. White, E. Petersen, J. Edgecumbe, G. Rakuljic, N. Satyan, A. Vasilyev, and A. Yariv, "A linearly chirped seed suppresses SBS in high-power fiber amplifiers, allows coherent combination, and enables long delivery fibers," Proc. SPIE **8961**, 896102 (2014).
12. T. Weyrauch, M. Vorontsov, J. Mangano, V. Ovchinnikov, D. Bricker, E. Polnau, and A. Rostov, "Deep turbulence effects mitigation with coherent combining of 21 laser beams over 7 km," Opt. Lett. **41**, 840–843 (2016).
13. N. Satyan, A. Vasilyev, G. Rakuljic, V. Leyva, and A. Yariv, "Precise control of broadband frequency chirps using optoelectronic feedback," Opt. Express **17**, 15991–15999 (2009).
14. V. Jayaraman, G. D. Cole, M. Robertson, C. Burgner, D. John, A. Uddin, and A. Cable, "Rapidly swept, ultra-widely-tunable 1060 nm MEMS-VCSELs," Electron. Lett. **48**, 1331–1333 (2012).
15. Agiltron, Inc., Woburn, Massachusetts, USA.
16. E. Petersen, Z. Y. Yang, N. Satyan, A. Vasilyev, G. Rakuljic, A. Yariv, and J. O. White, "Stimulated Brillouin scattering suppression with a chirped laser seed: comparison of dynamical model to experimental data," IEEE J. Quantum Electron. **49**, 1040–1044 (2013).
17. To avoid an initial spike in the SBS, it is important that the laser wave inside the fiber be chirped at $t = 0$.
18. P. D. Dragic, S. W. Martin, A. Ballato, and J. Ballato, "On the anomalously strong dependence of the acoustic velocity of alumina on temperature in aluminosilicate glass optical fibers–part I: material modeling and experimental validation," Int. J. Appl. Glass Sci. **7**, 3–10 (2016).
19. L. Thévenaz, A. Fellay, and W. Scandale, "Brillouin gain spectrum characterization in optical fibers from 1 to 1000 K," in *16th International Conference on Optical Fiber Sensors*, Nara, Japan, 13–17 October 2003.
20. M. Niklès, L. Thévenaz, and P. A. Robert, "Brillouin gain spectrum characterization in single-mode optical fibers," J. Lightwave Technol. **15**, 1842–1851 (1997).
21. A. Fellay, "Extreme temperature sensing using Brillouin scattering in optical fibers," Ph.D. thesis (Ecole Polytechnique Fédérale de Lausanne, 2003).
22. M. Hildebrandt, S. Büsche, P. Weßels, M. Frede, and D. Kracht, "Brillouin scattering spectra in high-power single-frequency ytterbium doped fiber amplifiers," Opt. Express **16**, 15970–15979 (2008).
23. Private communication, Andrew J. Stentz, LGS Innovations, Florham Park, New Jersey, USA (2012).